

## Adsorption mechanism of dodecyl phosphoric acid and dodecyl phosphate on kaolinite surface: DFT calculation and experimental verification

Shaowen Peng <sup>2</sup>, Lingyun Liu <sup>1,2</sup>, Chuilei Kong <sup>2</sup>, Fangqin Lu <sup>2</sup>, Hao Cheng <sup>2</sup>

<sup>1</sup> Joint National-Local Engineering Research Centre for Safe and Precise Coal Mining, Huainan 232001, China

<sup>2</sup> Department of Materials Science and Engineering, Anhui University of Science and Technology, Huainan 232001, China

Corresponding author: [lyunliu@163.com](mailto:lyunliu@163.com) (Lingyun Liu)

**Abstract:** To master the adsorption mechanism of dodecyl phosphoric acid (DDPA) and dodecyl phosphate (DPA) on the (001) and (00 $\bar{1}$ ) surfaces of kaolinite. Through density functional theory (DFT), the adsorption configurations of DDPA and DPA on the (001) and (00 $\bar{1}$ ) surfaces of kaolinite, the analysis of differential electron density, the charge transfer analysis of each bonding atom by Mulliken population, and the density of states analysis were studied and analyzed respectively, and flotation experiments were carried out for verification. The simulation results show that the adsorption energy of DDPA and DPA on the (001) surface of kaolinite is much stronger than that on the (00 $\bar{1}$ ) surface of kaolinite. According to the Mulliken bond population results, it indicates that DDPA forms effective hydrogen bonds on both the (001) surface of kaolinite and the (00 $\bar{1}$ ) surface of kaolinite, while DPA only forms strong hydrogen bonds on the (001) surface of kaolinite. The flotation results show that when the reagent concentration is lower than 1 mmol/L, DPA has a significant difference in the recovery performance of kaolinite and quartz of 125-75  $\mu\text{m}$ , DPA is more likely to selectively adsorb on the surface of kaolinite than DDPA, and in the kaolinite-quartz mixed mineral system, when the mineral particle size is 125-75  $\mu\text{m}$ , the selective adsorption effect of DPA on kaolinite is better, which is consistent with the theoretical results. Also, because the coal slime water produced during the wet coal washing and processing in the industrial process contains a large number of fine particles of kaolinite and quartz, it becomes possible to separate kaolinite in the coal slime water using DPA as a collector.

**Keywords:** dodecyl phosphoric acid, dodecyl phosphate, kaolinite, density functional theory, adsorption mechanism

### 1. Introduction

Kaolinite is one of the main components in coal slime water and has important uses in biology, environmental protection, new materials and other aspects (Li et al., 2023; Chi et al., 2017; Chen et al., 2017; Morsy et al., 2014; Müller et al., 2020). In the current process of wet coal washing and processing, a large amount of coal slime water is produced, and the coal slime water is mixed with a large number of fine particles of kaolinite. The existence of minerals such as kaolinite not only affects the yield and grade of flotation clean coal, but also seriously affects the dewatering of flotation tailings, which has also become a hot topic of concern for scholars. Therefore, the separation of kaolinite from coal slime water is of great significance for the clarification treatment of highly argillized coal slime water and the processing and utilization of kaolinite.

At present, fine kaolinite is mainly separated from minerals by flotation, so there are many studies on the collector reagents for kaolinite flotation (Zhou et al., 2022; Yang et al., 2014). In recent years, many scholars have studied the flotation behavior of kaolinite. Many researchers have been committed to studying and developing new types of cationic collectors to improve the flotation behavior of kaolinite. Among them, amine collectors have a better adsorption effect on kaolinite (Ma et al., 2009). Liu LY found through the research on the aggregation behavior of kaolinite particles by cationic, anionic and nonionic

surfactants that the aggregation effect of kaolinite particles in the presence of cationic surfactants was significantly better than that in anionic and nonionic surfactants, and the adsorption capacity of dodecylamine on the surface of kaolinite was greater than that of oleic acid (Liu et al., 2018). Liu et al. (2015) studied the effects of particle size and the chain length of reagents on the flotation of kaolinite by quaternary ammonium salt through flotation experiments. However, these reagents are mainly used for separating kaolinite in bauxite and not mainly for collecting kaolinite in coal slime water (Longhua et al., 2015).

The coal slime water mainly contains minerals such as kaolinite and quartz. Among them, the crystal structure of kaolinite is a triclinic system, with specific lattice constants and angles. The (001) and (001) planes of kaolinite are important surfaces of the kaolinite crystal (Ma et al., 2023; Šolc et al., 2011), and its crystal structure is composed of connected Si-O tetrahedra and Al-O octahedra, and the structural layers are stacked along the c-axis. The interlayers of kaolinite are strengthened by strong hydrogen bonds ( $O-OH = 0.289$  nm), and the stacking mode is that adjacent structural layers are mutually staggered by  $1/3a$  along the a-axis, with rotations at different angles, resulting in different polytypes of kaolinite. In the actual structure, due to the deformation of Al-OH and the difference in size from the Si-O tetrahedron, the tetrahedron must undergo a slight relative rotation and warping to adapt to the Al-OH sheet. The crystal structure of quartz is composed of Si-O tetrahedra, each Si atom is surrounded by four O atoms, and the tetrahedra are connected through the vertices to form a three-dimensional framework structure. The layered structural characteristics of kaolinite and quartz reflect the differences in their respective chemical compositions and crystal structures, resulting in differences in the surface properties of the two minerals.

Therefore, it is necessary to find a reagent that can perform targeted adsorption on the (001) surface of kaolinite and have no adsorption or weak adsorption on the (001) surface of kaolinite, which is of great significance for the separation of kaolinite from coal slime water. Studies have shown that phosphoric acid has a certain activation effect on the surface of kaolinite. The activation of phosphoric acid is used to replace the more commonly used polymerization of dehydrated kaolinite and undehydrated kaolinite (Zhang et al., 2020). Kaolinite has better floatability under neutral conditions, while quartz has better floatability at  $pH = 12$  (Ali et al., 2019; Zhou et al., 2022). Some ions such as  $Ca^{2+}$  have little effect on the floatability of kaolinite, but can improve the floatability of quartz at  $pH = 12$  (Hou et al., 2020). Liu's research shows that the higher the iron (Fe) content in kaolinite, the better the adsorption behavior of sodium oleate on kaolinite (Liu et al., 2024). The ACA study shows that kaolinite activated by phosphoric acid has higher reactivity and an increased specific surface area (Alvarez-Coscojuela et al., 2024). W Liu's research shows that the adsorption behavior of reagents on minerals is closely related to the charge size of the O atom on the reagent head group (Liu et al., 2019).

Therefore, in this thesis, DDPA and DPA were selected for flotation experiments. Experiments were carried out using different concentrations of reagents for minerals of different particle size grades, and the results were analyzed to confirm whether DDPA and DPA have selectivity for the flotation of kaolinite and quartz, thereby determining the application prospects of the reagents for the recovery of kaolinite.

## 2. Sample preparation and test methods

### 2.1. Material preparation

The high-purity kaolinite and quartz used in the experiment were respectively from Huaibei Jinyan Coal Measures Kaolin Co Ltd in Anhui Province and Henan Minghai Environmental Protection Technology Co Ltd. The mineral samples were crushed, ground and sieved, and then four particle size grades of 500 - 250 $\mu$ m, 250 - 125 $\mu$ m, 125 - 75 $\mu$ m and 75 - 45 $\mu$ m were obtained respectively for the experiment.

DPA was purchased from Jiangsu Aikon Biopharmaceutical R&D Co Ltd in China, and DDPA was purchased from Shanghai Macklin Biochemical Technology Co Ltd in China. All the reagent solutions in the experiment were freshly prepared and used immediately. The prepared reagent concentration was  $1 \times 10^{-2}$  mol/L, and it was stored in a brown frosted glass bottle in a cool place. During use, the concentration of the mixed solution was controlled by adding different volumes. All the water used in the experiment was deionized water.

## 2.2. Test method

### 2.2.1. Single mineral flotation test

In this experiment, the XFG-35II type flotation machine produced by Changsha Instrument and Equipment Co Ltd. Was used. For each group of experiments,  $10.000 \pm 0.001$  g of kaolinite and quartz samples were weighed respectively using an analytical balance and placed into the flotation cell. Then, the corresponding volume of deionized water was added to the flotation cell. After adding the deionized water, the mixture was stirred for 2 minutes on the flotation machine to evenly disperse the minerals in the water. The DDPA and DPA collectors were added respectively, and then the solutions were made to reach different concentrations. After adding the collectors, the mixture was stirred for 3 minutes to fully mix the minerals and the reagents. Then, the aeration valve of the flotation machine was opened to start froth scraping, and the froth scraping time was 3 minutes. The rotation speed of the flotation machine was 2400 r/min. After the flotation, the concentrate and tailings were dried and weighed. The recovery rate calculation formula is as follows:

$$P = \frac{m_1}{m_1 + m_2} \times 100\% \quad (1)$$

In the formula: P represents the flotation yield, %;  $m_1$  is the mass of the concentrate, g;  $m_2$  is the mass of the tailings, g.

### 2.2.2. Flotation test of kaolinite - quartz mixed minerals

The operation steps of the flotation test of the kaolinite-quartz mixed system are as follows: Firstly, the two minerals are mixed in different proportions. The percentage of kaolinite is determined according to the aluminum-silicon ratio in the mixed sample. The flotation steps are the same as those of the single mineral, and the calculation of the flotation recovery rate is also the same as that of the single mineral flotation recovery rate. In the kaolinite-quartz mixed mineral system, the grade of the flotation concentrate is mainly judged by different proportions. The specific operations are as follows:

A series of kaolinite-quartz mixed samples with different proportions were respectively configured. XRF analysis was conducted on each sample to determine the contents of  $\text{Al}_2\text{O}_3$  and  $\text{SiO}_2$ . The standard curve diagram of concentrate grade was obtained by using the ratio of  $\text{Al}_2\text{O}_3/\text{SiO}_2$  and the content of kaolinite-quartz, as shown in Fig. 1. Next, a kaolinite-quartz mixed sample with a mass ratio of 1:1 was configured. Flotation tests of DDPA and DPA in the kaolinite-quartz mixed system were carried out at different concentrations of 1 mmol/L, 2 mmol/L, 3 mmol/L, 4 mmol/L, and 5 mmol/L. XRF analysis was respectively conducted on the flotation concentrates to determine the contents of  $\text{Al}_2\text{O}_3$  and  $\text{SiO}_2$ . Then, the mass percentage of kaolinite in the flotation concentrate, that is, the grade of the flotation concentrate, was determined according to the corresponding standard curve based on the ratio of  $\text{Al}_2\text{O}_3/\text{SiO}_2$ .

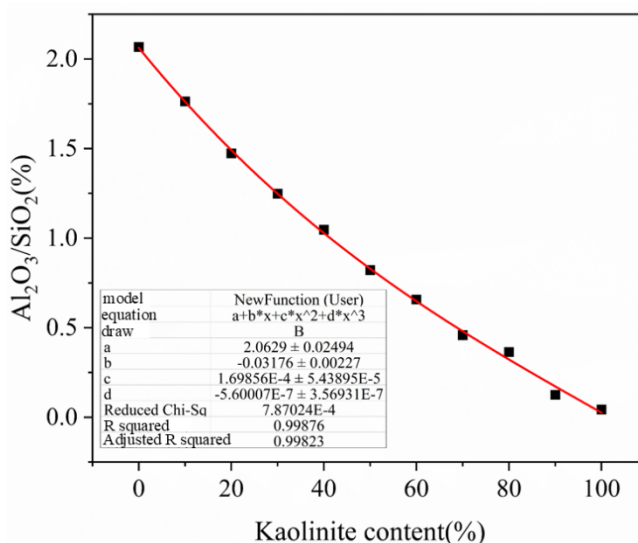


Fig. 1. The standard curve of concentrate grade in the kaolinite - quartz system

### 2.2.3. Fourier Transform Infrared Spectroscopy (FTIR)

The FTIR spectra of the samples were measured at room temperature ( $25 \pm 2$  °C) using a Nicolet 740 FTIR spectrometer in the wavenumber range of 400 to 4000  $\text{cm}^{-1}$  on KBr pellet. Before the measurement, kaolinite and quartz were ground to  $< 15$   $\mu\text{m}$  using an agate mortar. Then, 1 g of the sample was added to 30 mL of aqueous solution with or without 33.33 mg/L DPA at a pH value of 6.65 and adjusted for 0.5 h. Subsequently, the samples were filtered, washed three times with deionized water, and dried in a vacuum oven at 35°C for 24 hours.

## 3. Simulation calculation

### 3.1. Computational details

The density functional calculations of DDPA and DPA on different layers of kaolinite were performed using the CASTEP module in Materials Studio 2019 software. The exchange-correlation function for the lattice geometry optimization of the kaolinite bulk phase was the GGA-PBE function, and the plane wave cutoff energy was set to 400 eV. The ultrasoft pseudopotential was used to describe the interaction between valence electrons and ions. The BFGS algorithm was used to optimize and calculate the properties of the model, and the self-consistent field convergence accuracy was set to  $2.0 \times 10^{-6}$  eV/atom. The van der Waals force in the density functional calculation process was corrected using the Tkatchenko-Scheffler (TS) method. The convergence criteria for geometric optimization: the maximum atomic displacement was 0.2 pm, the interatomic force was 0.05 eV/Å, the interatomic internal stress was 0.1 GPa, the total energy change of the system was  $2.0 \times 10^{-5}$  eV/atom, and the smearing value used for the density of states analysis was 0.2 eV; all calculations were performed in the reciprocal space. OTAC+ was placed in a 2 nm×2 nm×4 nm periodic unit cell for optimization, and the Gamma point was selected for the Monkhorst-Pack grid k-point (Clark et al., 2005; Segall et al., 2002). Since the 00-1 surface structure of kaolinite is similar to that of quartz, the adsorption effect of the reagent on the 00-1 surface of kaolinite was used to replace the adsorption effect of the reagent on quartz in this paper. The initial adsorption sites of different kaolinite layers are shown in Fig. 2. There are a total of three main adsorption regions (H1, H2, H3). According to the structural characteristics of the reagent head group, each adsorption site can be divided into three adsorption modes according to different rotation angles of the reagent, so there are a total of nine adsorption sites, namely H1-1, H1-2, H1-3, H2-1, H2-2, H2-3, H3-1, H3-2, and H3-3.

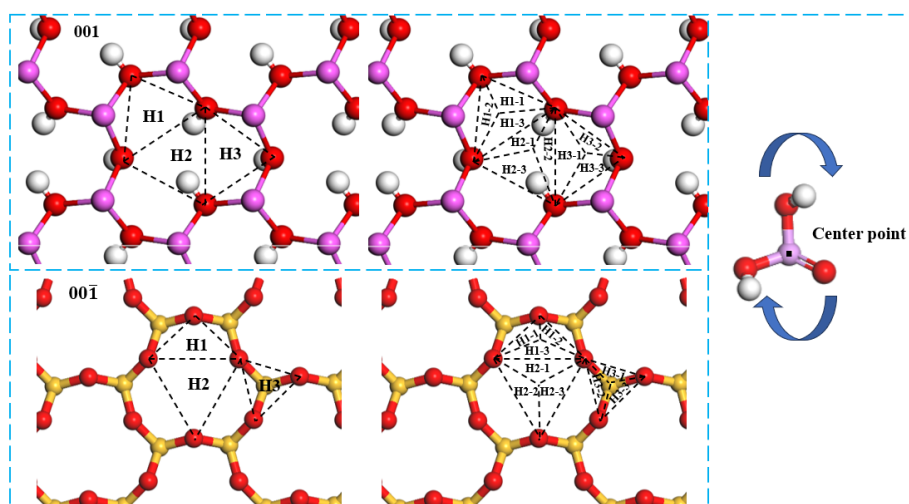


Fig. 2. Construction of adsorption sites of the (001) surface and (001̄) surface model of kaolinite

### 3.2. Model construction

#### 3.2.1. The characteristics of DDPA and DPA

The Mulliken atomic partial charges of DDPA and DPA are presented in Fig. 3. The data reveal that DDPA contains three highly electronegative oxygen atoms with charges of O (-0.663e), O (-0.580e), and

O (-0.571e), whereas DPA has four such oxygen atoms with charges of O (-0.659e), O (-0.603e), O (-0.554e), and O (-0.568e). Electronegative atoms play a crucial role in electrostatic adsorption. Additionally, the polar group  $-\text{PO}_3\text{H}^{2+}$  in DDPA carries a charge of +0.105e, while the  $-\text{PO}_4\text{H}^{2+}$  group in DPA has a charge of -0.352e. Preliminary analysis indicates that both agents may primarily adsorb onto mineral surfaces via electrostatic interactions and hydrogen bonding.

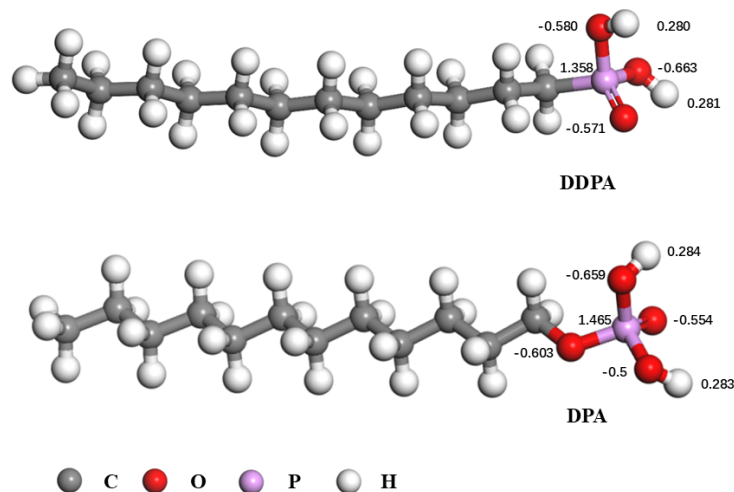


Fig. 3. Molecular structures of DDPA and DPA

## 4. Results and discussion

### 4.1. Simulation calculation

#### 4.1.1. Adsorption energy and stable adsorption configuration

As shown in Table 1 and Table 2, the adsorption energies of DDPA and DPA on the (001) and (00 $\bar{1}$ ) surfaces of kaolinite are presented respectively. The lower the adsorption energy, the better the adsorption effect. It can be seen from Table 1 that the adsorption energies of DDPA on the (001) surface of kaolinite are all lower than -95.736 kJ/mol, and the adsorption energies at 6 adsorption sites are lower than -112.2344 kJ/mol. Among them, the adsorption energy at the adsorption site H2-1 is the lowest, which is -147.9216 kJ/mol. While the lowest adsorption energy of DDPA on the H3-1 adsorption site on the (00 $\bar{1}$ ) surface of kaolinite is -47.4288 kJ/mol. On the whole, the adsorption energies at each adsorption site are much greater than those on the (001) surface of kaolinite. It can be seen from Table 2 that the adsorption energies of DPA on the (001) surface of kaolinite are all lower than -81.1814 kJ/mol, and the adsorption energies at 7 adsorption sites are lower than -122.4806 kJ/mol. Among them, the lowest adsorption energy at the adsorption site H3-1 is -152.375 kJ/mol. While the lowest adsorption energy of DPA on the (00 $\bar{1}$ ) surface of kaolinite is at the H2-1 site, which is -46.7846 kJ/mol. On the whole, each adsorption energy is much greater than that on the (001) surface of kaolinite. It can be seen that the adsorption of DDPA and DPA on the (001) surface of kaolinite is much stronger than that on the (00 $\bar{1}$ ) surface.

Table 1. Adsorption energy of DDPA on the (001) and (00 $\bar{1}$ ) surfaces of kaolinite

DDPA Adsorption site	Adsorption energy (kJ/mol)				
	001	00 $\bar{1}$	Adsorption site	001	00 $\bar{1}$
H1-1	-130.4784	-31.08	H2-3	-112.2344	-45.7296
H1-2	-95.7360	-30.1584	H3-1	-122.5296	-47.4288
H1-3	-126.0432	-31.6848	H3-2	-99.2336	-43.4448
H2-1	-147.9216	-42.2024	H3-3	-96.5872	-37.3680
H2-2	-134.5872	-44.0304			

Table 2. Adsorption energy of DPA on the (001) and (00 $\bar{1}$ ) surfaces of kaolinite

DPA		Adsorption energy (kJ/mol)			
Adsorption site	001	00 $\bar{1}$	Adsorption site	001	00 $\bar{1}$
H1-1	-140.9126	-45.3158	H2-3	-81.1814	-37.9142
H1-2	-129.6518	-32.0390	H3-1	-152.375	-35.0918
H1-3	-124.5254	-29.1590	H3-2	-137.8214	-38.8262
H2-1	-122.4806	-46.7846	H3-3	-95.7446	-28.7174
H2-2	-139.1238	-31.9238			

The stable adsorption configurations of DDPA at the optimal adsorption site H2-1 on the (001) surface of kaolinite and at the optimal adsorption site H3-1 on the (00 $\bar{1}$ ) surface are shown in Fig. 4. For the hydrogen bond analysis, it can be seen that on the (001) surface of kaolinite, DDPA is mainly adsorbed by forming three hydrogen bonds through the O atoms in the molecule and the H atoms on the surface of the Al-OH group, namely O145-H15, O146-H34 and O84-H90. While on the (00 $\bar{1}$ ) surface of kaolinite, it is mainly adsorbed by forming two hydrogen bonds through the H atoms in the DDPA molecule and the O atoms on the Si-O group, namely O39-H58 and O41-H59.

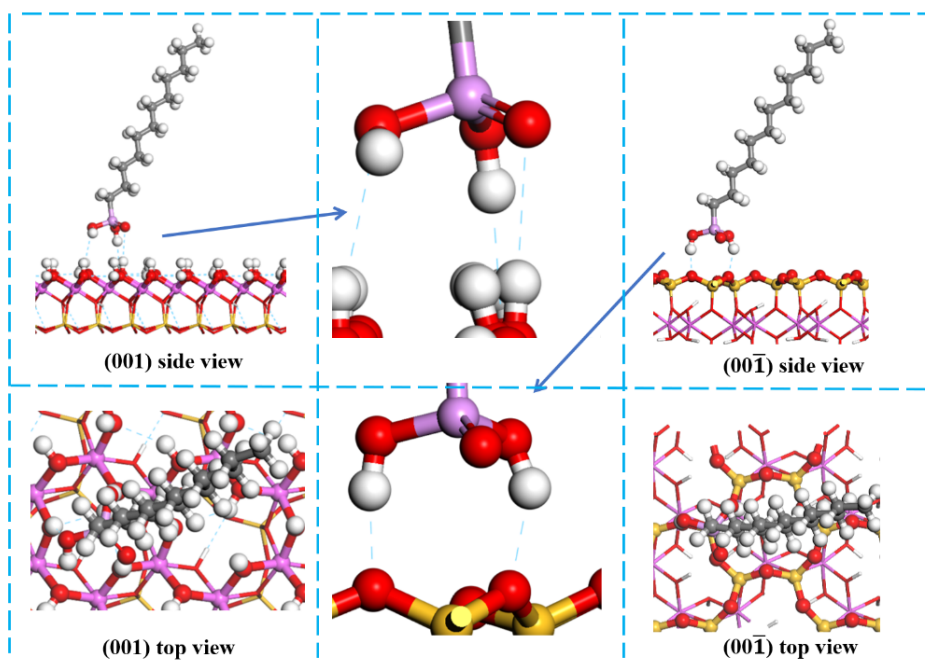


Fig. 4. The optimal adsorption configuration of DDPA on the surface of kaolinite

The stable adsorption configurations of DPA at the optimal adsorption site H3-1 on the (001) surface of kaolinite and at the optimal adsorption site H2-1 on the (00 $\bar{1}$ ) surface are shown in Fig. 5. The hydrogen bond analysis shows that on the (001) surface of kaolinite, DPA is mainly adsorbed by forming three hydrogen bonds through the O atoms in the molecule and the H atoms on the Al-OH group, namely O31-H33, O73-H22, and O74-H11. While on the (00 $\bar{1}$ ) surface of kaolinite, it is mainly adsorbed by forming one hydrogen bond through the H atom in the DPA molecule and the O atom on the Si-O group, which is O28-H34.

It can be known from the analysis of adsorption energy and hydrogen bonds that the adsorption of DPA on the (001) surface of kaolinite is better than that of DDPA, while the adsorption on the (00 $\bar{1}$ ) surface of kaolinite is weaker than that of DDPA. Therefore, in conclusion, both DDPA and DPA have targeted adsorption capabilities on the (001) surface of kaolinite, but the adsorption ability of DPA is stronger than that of DDPA.

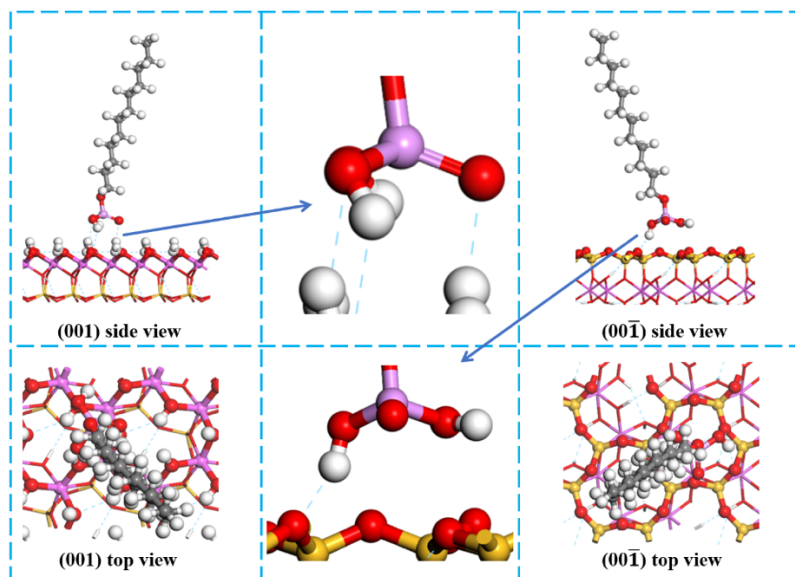


Fig. 5. The optimal adsorption configuration of DPA on the surface of kaolinite

#### 4.1.2. Analysis of differential electron density, Mulliken population and density of states

In order to further analyze the adsorption mechanism of DDPA and DPA on the AL-OH group of kaolinite (001) surface and the Si-O group of kaolinite (00 $\bar{1}$ ), the differential electron density, Mulliken population and density of states analysis were carried out for the optimal adsorption configuration of the two agents on the kaolinite surface. Figs. 6 and 7 are the differential electron density diagrams of the adsorption of DDPA and DAP on the (001) surface and (00 $\bar{1}$ ) surface of kaolinite. The blue area indicates the accumulation of electrons, and the yellow area indicates the consumption of electrons.

As shown in Fig. 6, obvious electron transfer exists on both the (001) surface and the (00 $\bar{1}$ ) surface of kaolinite for DDPA. During the adsorption process of DDPA on the (001) surface of kaolinite, electrons mainly accumulate at the double-bond O atoms in the DDPA molecule, while during the adsorption process on the (00 $\bar{1}$ ) surface, electrons mainly concentrate at the O atoms of the Si-O group. The electron transfer situation during the adsorption process of DPA on the (001) surface and the (00 $\bar{1}$ ) surface of kaolinite is basically consistent with that of DDPA (Fig. 7).

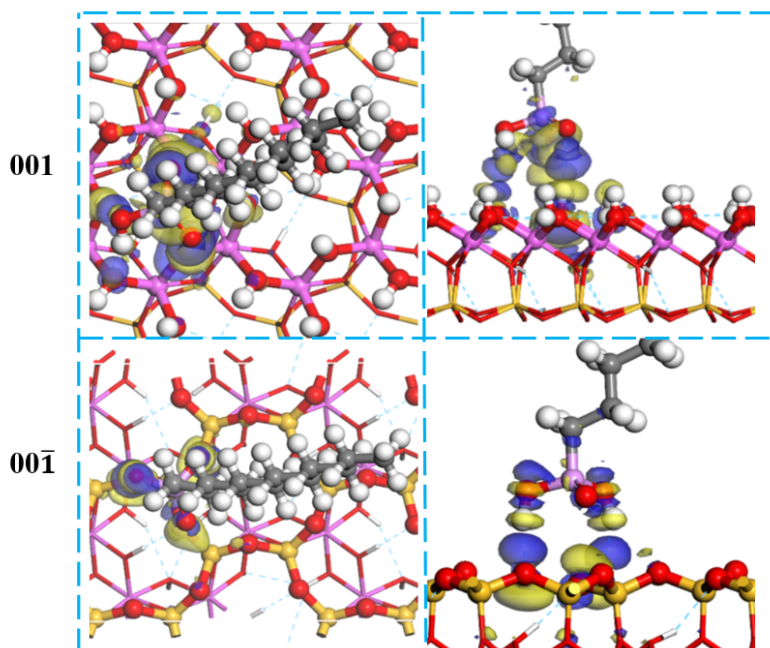


Fig. 6. The differential electron density map of DDPA adsorption on the surface of kaolinite

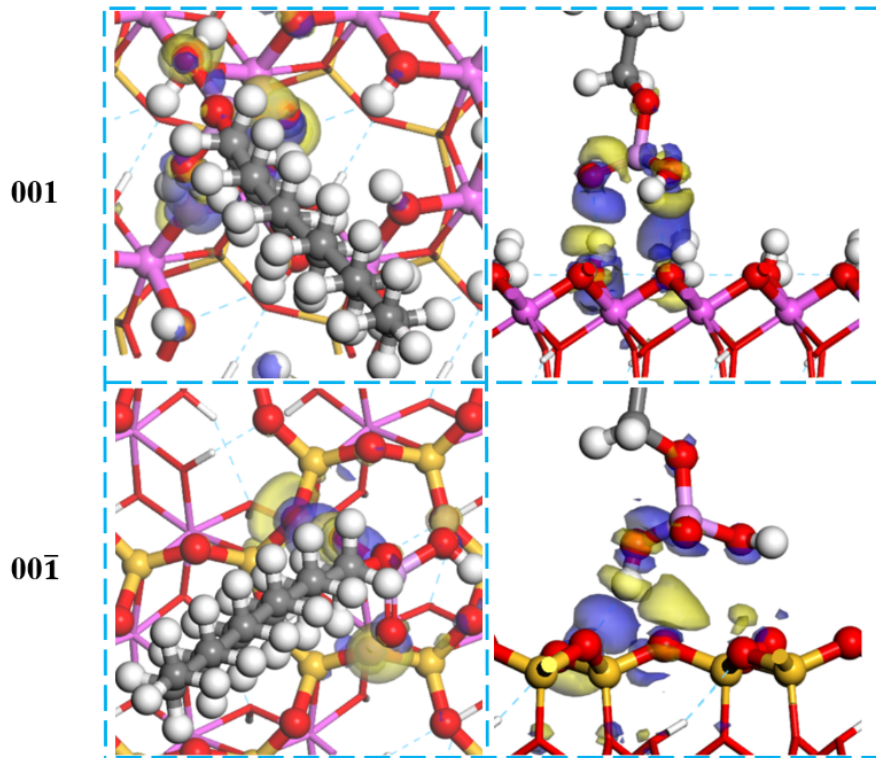


Fig. 7. The differential electron density map of DPA adsorption on the surface of kaolinite

Table 3. Mulliken charge transfer of the reagent before and after adsorption on the (001) surface of kaolinite

Collector type	Atom number	Adsorption State	Charge(e)	Transfer
DPA	O <sub>74</sub>	before	-1.00	0.04
		after	-0.96	
	H <sub>33</sub>	before	0.25	-0.25
		after	0.5	
	O <sub>73</sub>	before	-1	-0.02
		after	-1.02	
	H <sub>22</sub>	before	0.45	-0.02
		after	0.43	
	H <sub>11</sub>	before	0.45	-0.02
		after	0.43	
O <sub>31</sub>	before	-1.06	0.02	
	after	-1.04		
DDPA	O <sub>145</sub>	before	-1	-0.03
		after	-1.03	
	H <sub>90</sub>	before	0.25	-0.25
		after	0.5	
	O <sub>146</sub>	before	-0.99	0.04
		after	-0.95	
	H <sub>7</sub>	before	0.45	-0.02
		after	0.43	
	H <sub>3</sub>	before	0.41	-0.04
		after	0.45	
O <sub>15</sub>	before	-1.06	0.06	
	after	-1		

Table 4. Mulliken charge transfer of the reagent before and after adsorption on the (00 $\bar{1}$ ) surface of kaolinite

Collector type	Atom number	Adsorption State	Charge(e)	Transfer
DPA	O <sub>28</sub>	before	-1.14	0.01
		after	-1.13	
	H <sub>34</sub>	before	0.25	-0.25
		after	0.5	
DDPA	O <sub>39</sub>	before	-1	-0.13
		after	-1.13	
	H <sub>58</sub>	before	0.25	0.25
		after	0.5	
	O <sub>41</sub>	after	-1.03	-0.13
		before	-1	
	H <sub>59</sub>	after	-1.13	0.25
		before	0.25	
		after	0.5	

Charge redistribution is one of the main reasons for the formation of hydrogen bonds. Therefore, in the study of the adsorption process of the reagent on the kaolinite surface, the charge distribution was used to study the charge redistribution of the single-bond O atoms, double-bond O atoms, and H atoms in the adsorption process. Tables 3 and 4 show the Mulliken charge transfer before and after the adsorption of the reagent on the (001) surface and (00 $\bar{1}$ ) surface of kaolinite, respectively. It can be seen that when the reagent is adsorbed on the (001) surface of kaolinite, the double-bond O74 atom in DPA gains 0.04e electrons after adsorption, the single-bond O73 atom loses 0.02e, the H33 atom loses a total of 0.25e, the O31 on the kaolinite surface gains 0.02e, and both H22 and H11 lose 0.02e; in DDPA, the double-bond O145 atom loses 0.03e electrons after adsorption, the single-bond O146 atom gains 0.04e, the H90 atom loses a total of 0.25e, the O15 on the kaolinite surface gains 0.06e, and H3 and H7 lose 0.04e and 0.02e, respectively; when the reagent is adsorbed on the (00 $\bar{1}$ ) surface of kaolinite, the H34 atom in DPA loses 0.25e electrons after adsorption, and the O28 on the kaolinite surface gains 0.01e electrons; in DDPA, the H58 and H58 atoms gain 0.25e electrons after adsorption, and the O39 and O41 on the kaolinite surface lose 0.13e electrons; The electron transfer between atoms forms hydrogen bonds, which plays a certain role in the stability of the reagent adsorption.

Table 5. Mulliken population of the reagent on the (001) surface of kaolinite

Adsorption configuration	Bond type	Population	Length
DDPA	O145-H15	0.08	1.80824
	O146-H34	0.03	1.96126
	O84-H90	-0.01	2.84844
DPA	O31-H33	0.04	1.96424
	O73-H22	0.04	1.98202
	O74-H11	-0.02	2.36973

Table 6. Mulliken population of the reagent on the (00 $\bar{1}$ ) surface of kaolinite

Adsorption configuration	Bond type	Population	Length
DDPA	O39-H58	0.04	1.88093
	O41-H59	0.02	2.00682
DPA	O28-H34	0	2.75849

Tables 5 and 6 respectively show the Mulliken populations of hydrogen bonds formed after the adsorption of DPA and DDPA on the kaolinite (001) surface and the kaolinite (00 $\bar{1}$ ) surface. The overlap population is inversely proportional to the bond length. When the overlap population is positive, it indicates that there is a driving force for active combination between the two atoms. The calculation results show that DDPA forms effective hydrogen bonds on both the kaolinite (001) surface and the kaolinite (00 $\bar{1}$ ) surface, while DPA only forms a strong hydrogen bond on the kaolinite (001) surface.

DDPA and DPA may interact with kaolinite surfaces via electrostatic forces, hydrogen bonds, or chemical bonds. During the adsorption process of reagent molecules onto the mineral surface, the molecular orbitals of the reagents hybridize with the electronic states of the mineral surface. Additionally, the formation of hydrogen bonds results in the redistribution of electron density.

The polar head groups of DDPA and DPA consist of single-bonded oxygen atoms, double-bonded oxygen atoms, phosphorus atoms, and hydrogen atoms. To investigate the reactivity of the double-bonded oxygen atoms in these collectors, we performed density of states (DOS) calculations using parameters consistent with those used for geometric structure optimization. The DOS analysis results are presented in Figs. 8 and 9, where the Fermi level ( $E_f$ ) is set to 0 eV.

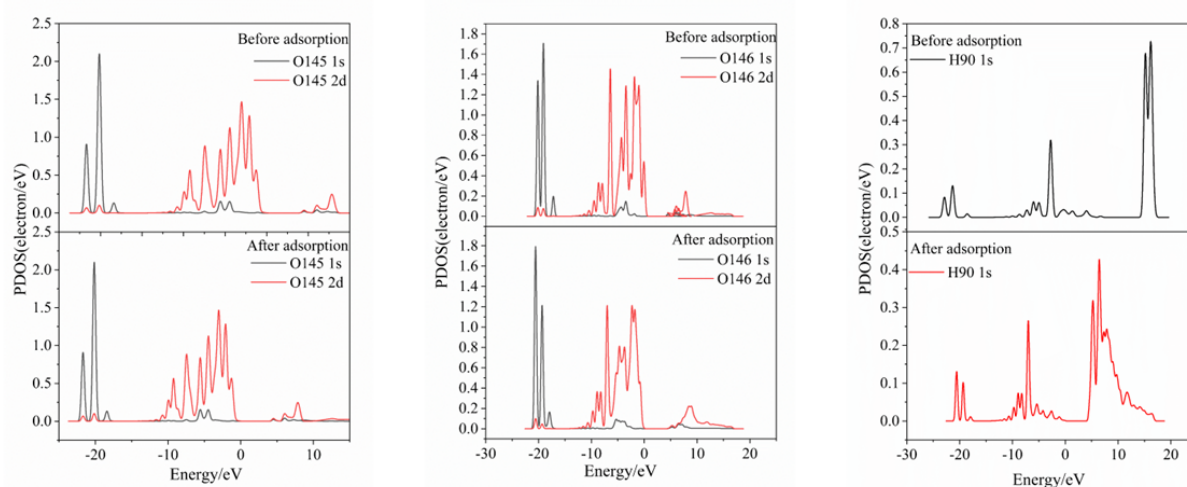


Fig. 8. The electronic density of states of DDPA before and after adsorption on the (001) surface of kaolinite

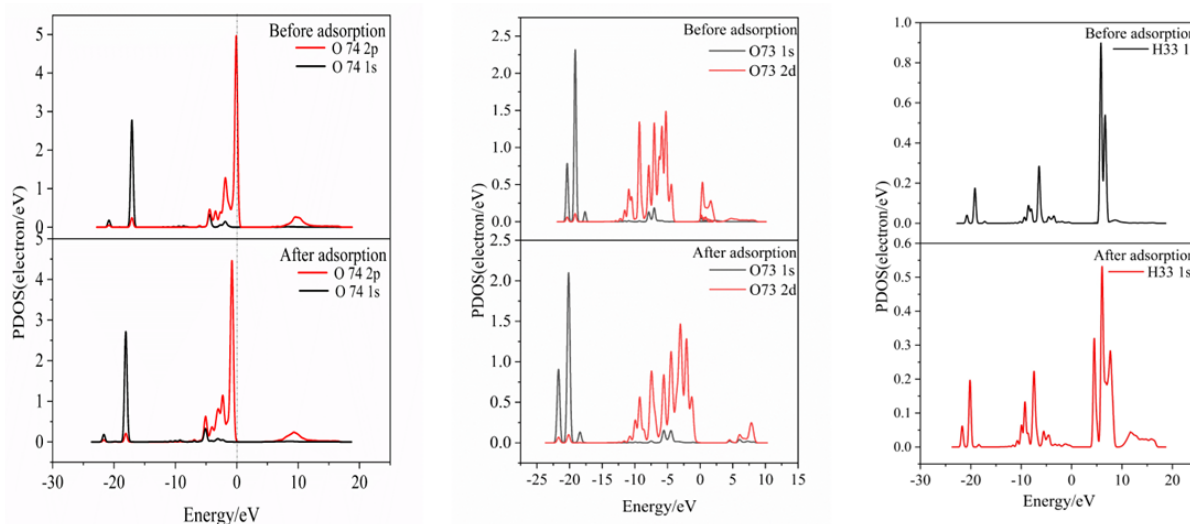


Fig. 9. The electronic density of states of DPA before and after adsorption on the (001) surface of kaolinite

According to the analysis of the density of states (DOS), it is evident that among the hydrogen bonds formed by DDPA, the O145-H15 bond exhibits a shorter length and stronger interaction, with a DOS value of 1.5 electrons/eV at the Fermi level. For DPA, both O31-H33 and O73-H22 exhibit shorter bond lengths and stronger interactions; however, the DOS value at the Fermi level for H33 after adsorption

remains unchanged at 0.9 electrons/eV. This indicates a significant decrease in the DOS of H atoms near the Fermi level, leading to reduced reactivity and weakened hybridization effects. The DOS values before and after the adsorption of both agents on the quartz (001) surface show no significant changes, suggesting the absence of chemical adsorption. These findings from the DOS analysis are consistent with the calculated and analyzed results of adsorption energy.

## 4.2. Experimental verification

### 4.2.1. Fourier transform infrared spectroscopy analysis

At present, it is difficult to directly verify the adsorption differences of the reagent on the kaolinite (001) surface and the kaolinite (00 $\bar{1}$ ) surface by experimental means. Since the quartz mineral is similar to the kaolinite (00 $\bar{1}$ ) surface structure in crystal structure, both are Si-O basal planes. Therefore, the paper used quartz and kaolinite minerals for infrared spectral analysis after reagent adsorption, and carried out flotation tests of single minerals and mixed minerals respectively to verify the previous simulation results.

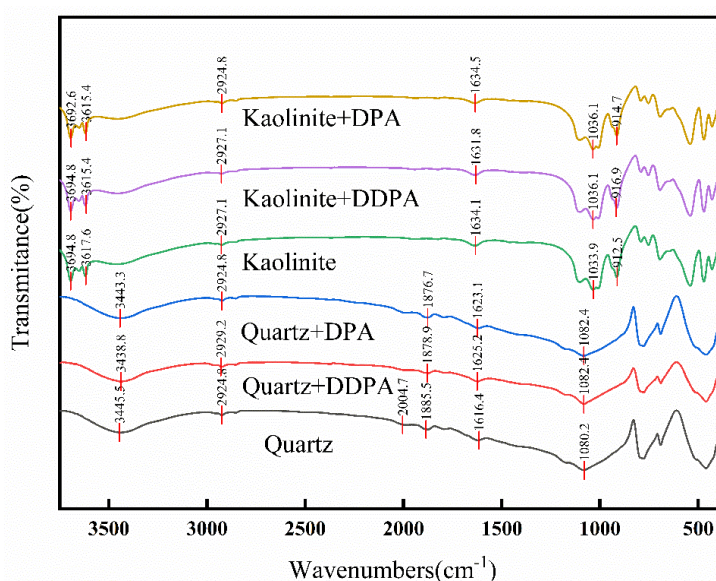


Fig. 10. Infrared spectra of DDPA and DPA before and after their interaction with kaolinite and quartz (reagent concentration =  $3 \times 10^{-4}$  mol/L)

The infrared spectra of DDPA and DPA before and after adsorption on the surfaces of kaolinite and quartz are shown in Fig. 10. It can be seen that no new peaks appeared on the surfaces of kaolinite and quartz after the adsorption of the reagents, indicating that only physical adsorption occurred. Among them, after the interaction of quartz with DPA and DDPA, compared with the spectrum of quartz itself, there were shifts at 3445, 1885, and 1616, corresponding to the stretching motion of the carbon-hydrogen bond (C-H) and the bending motion of P=O respectively. After the interaction of DDPA and quartz, it shifted to a lower frequency at approximately 1885, indicating that the adsorption of the reagent on the quartz surface was weak. After the interaction of kaolinite with DPA, compared with its own spectrum, there was a shift at 3617, which was the result of the hydrogen bond interaction between the reagent and the surface of kaolinite; the shift at 1634 was caused by the stretching vibration of P=O and the bending motion of P=O, and shifted to the right.

### 4.2.2. Single mineral flotation test

The flotation characteristics of kaolinite and quartz minerals with DDPA and DPA at the natural pH value were studied, and the results are shown in Fig. 11. It can be seen that when the mineral particle size is less than 125  $\mu\text{m}$ , the adsorption effect of DPA on kaolinite and quartz is better than that of DDPA. However, when the concentration of DDPA is around 1 mmol/L, the flotation effect on minerals is

almost zero, while DPA still has a strong adsorption effect on kaolinite at a lower concentration. As shown in Fig. 12, when the reagent concentration is less than 1 mmol/L, DPA has a strong difference in the recovery performance of 125-75  $\mu\text{m}$  kaolinite and quartz. Therefore, at low concentrations, DPA is more likely to adsorb on the surface of kaolinite than DDPA. At high concentrations, the difference in the recovery performance of DPA and DDPA on kaolinite and quartz decreases. When the reagent concentration is greater than 2 mmol/L, the collection difference of DPA on kaolinite and quartz changes, and its collection performance on kaolinite is weaker than that of DDPA.

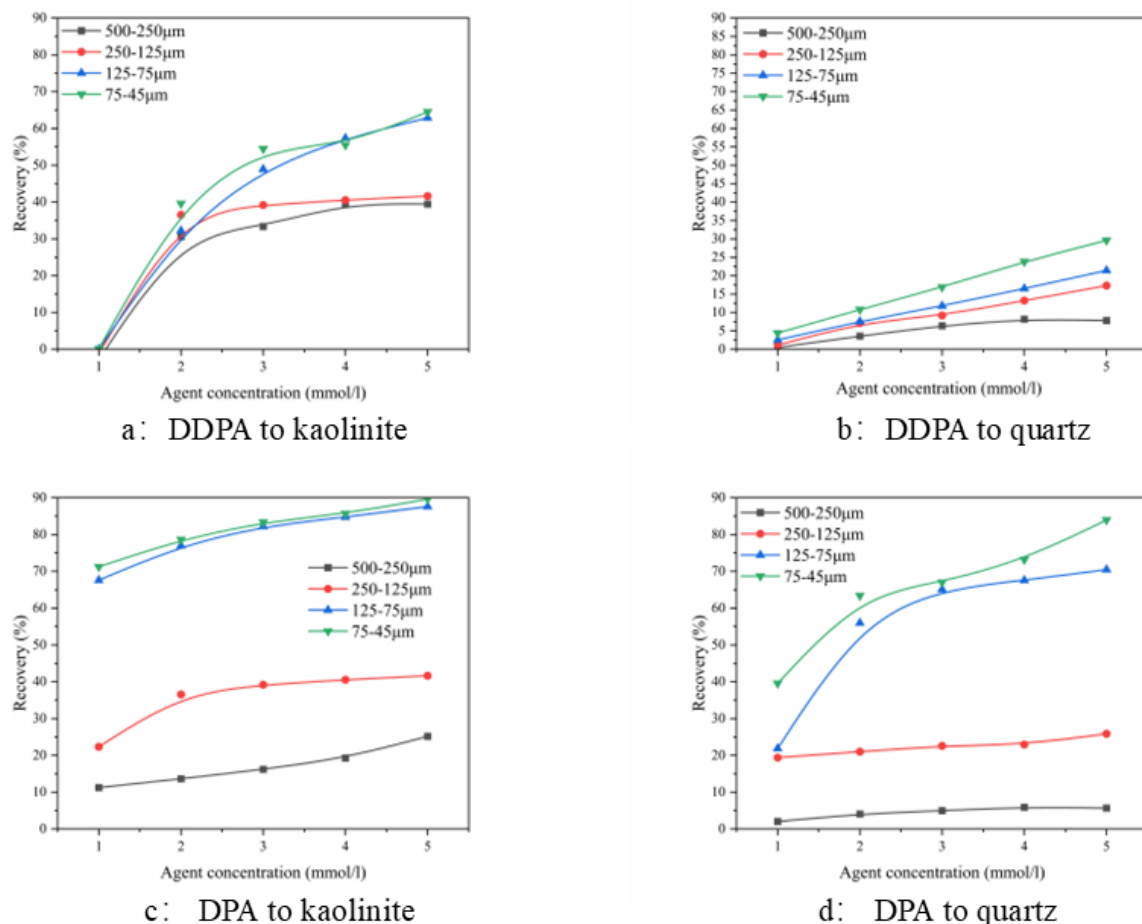


Fig. 11. The flotation performance of DDPA and DPA on kaolinite and quartz particles of different particle sizes

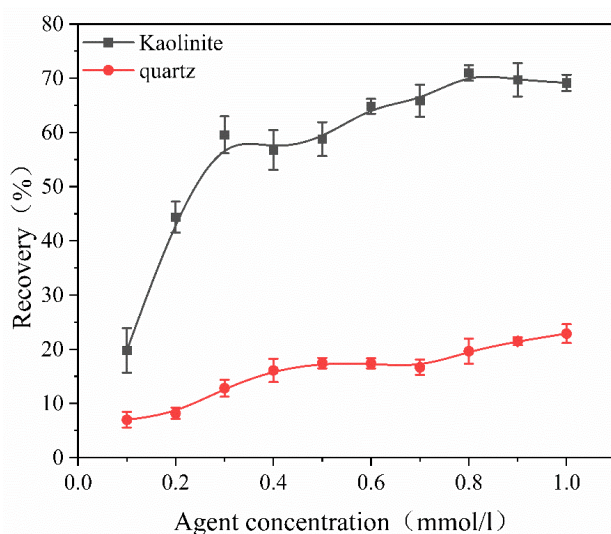


Fig. 12. The influence of DPA concentration on the recovery rates of 125 - 75  $\mu\text{m}$  kaolinite and quartz

### 4.2.3. Flotation test of mixed minerals

According to the flotation results of single minerals, the DPA reagent was selected in this paper, and the flotation test of kaolinite-quartz mixed minerals with a particle size of 125-75  $\mu\text{m}$  was carried out. The results are shown in Table 7.

Table 7. Test results of flotation separation of DPA and kaolinite-quartz (125 - 75  $\mu\text{m}$ ) mixed minerals under different concentrations

Agent	Agent concentration (mmol/L)	$\text{Al}_2\text{O}_3/\text{SiO}_2$ (%)	Separating efficiency (%)
DPA	1	54.32	68.62
	2	52.75	67.05
	3	49.11	63.41
	4	44.98	59.28
	5	44.66	58.96

It can be seen that when the mineral particle size is within 125 - 75  $\mu\text{m}$ , in the kaolinite - quartz mixed mineral system of DPA, when the reagent concentration is 1 mmol/L, the selective adsorption effect on kaolinite is the best, and the separation efficiency is 68.62%. With the increase of the concentration, the selective adsorption effect on kaolinite gradually decreases. When the reagent concentration is 5 mmol/L, the separation efficiency is 58.96%, which is consistent with the results of the single mineral flotation test. At the same time, it also indicates that the adsorption effect of DPA on the (001) surface of kaolinite is stronger than that on the (00 $\bar{1}$ ) surface of kaolinite.

## 5. Conclusions

By combining theoretical analysis and experimental verification methods, the adsorption characteristics of DPA and DPA on the (001) surface of kaolinite and the (00 $\bar{1}$ ) surface of kaolinite were studied. Flotation experiments showed that DPA and DPA exhibited different adsorption capacities (kaolinite > quartz), and when DPA was in the lower concentration range (< 1 mmol/l), the selective flotation separation of kaolinite could be carried out. When the concentration was in the range of 0.3 - 1 mmol/l, the recovery rate of kaolinite was between 63.35% and 67.59%, and the recovery rate of quartz was between 12.76% and 21.87%, indicating that this reagent has certain prospects as a collector for kaolinite. In the mixed mineral test, when the minerals were in the particle size range of 125 - 75  $\mu\text{m}$ , DPA also had certain selectivity for kaolinite. The results of adsorption energy, differential electron density analysis and Fourier transform infrared spectroscopy analysis indicated that the adsorption effect was achieved through hydrogen bonds and electrostatic interactions. The reason why the adsorption effect of DPA was better than that of DPA was due to the charge carried by the polar head group functional group of it. The electrostatic interaction was greater than that of DPA, and the electronegative atoms of the head group of the reagent were the key factors for electrostatic adsorption. Moreover, according to Mulliken population, it could be seen that because DPA formed a relatively stable hydrogen bond on the (00 $\bar{1}$ ) surface of kaolinite, its selective adsorption effect on kaolinite was weakened. At the same time, the hydrogen bonds formed by DPA on the kaolinite (001) surface were more than those formed on the kaolinite (00 $\bar{1}$ ) surface. Whether there were hydroxyl groups was the main difference between the surfaces of kaolinite and quartz, and it was also the main reason affecting the formation of hydrogen bonds and resulting in different adsorption effects. In conclusion, it can be seen that DPA has broad application prospects for the flotation of kaolinite.

## References

- ALI A.M., PADMANABHAN E., MIJINYAWA A., et al. 2019. *Effect of pH on the stability of quartz in a multi-phase system of kaolinite, hydrous Al (hydr) oxide and quartz*. SN Applied Sciences, 1: 1-11.
- ALVAREZ-COSCOJUELA A., MAÑOSA J., FORMOSA J., et al. 2024. *Structural characterisation and reactivity measurement of chemically activated kaolinite*. Journal of Building Engineering, 87: 109051.

- CHEN S., YANG Z., WANG F. 2019. *Preparation and characterization of polyimide/kaolinite nanocomposite films based on functionalized kaolinite*. Polymer Engineering & Science, 59(s2): E380-E386.
- CHI Q., ZHEN R., WANG X., et al. 2017. *The role of exfoliated kaolinite on crystallinity, ion conductivity, thermal and mechanical properties of poly (ethylene oxide)/kaolinite composites*. Polymer Bulletin, 74: 3089-3108.
- CLARK S.J., SEGALL M.D., PICKARD C.J., et al. 2005. *First principles methods using CASTEP*. Zeitschrift für kristallographie-crystalline materials, 220(5-6): 567-570.
- HOU B., LIU L. 2020 *Study on the influence of Ca<sup>2+</sup> in sodium oleate system on the flotation of kaolinite and quartz at different pH values*. Coal Engineering, 2020.
- LI Y., HOU D., DING X., et al. 2023. *Influence of coal-measure kaolinite with different types on the preparation of kaolinite nanotube*. Applied Clay Science, 246: 107179.
- LIU L., KONG C., ZHAO H., et al. 2024. *Elucidating the enhancement of kaolinite flotation by iron content through density functional theory: A study on sodium oleate adsorption efficiency*. International Journal of Mining Science and Technology, 34(6): 855-866.
- LIU W., LIU W., ZHAO B., et al. 2019. *Novel insights into the adsorption mechanism of the isopropanol amine collector on magnesite ore: A combined experimental and theoretical computational study*. Powder Technology, 343: 366-374.
- LIU L., SHEN L., LI W., et al. 2018. *Study on the aggregation behavior of kaolinite particles in the presence of cationic, anionic and non-ionic surfactants*. Plos one, 13(9): e0204037.
- LIU J., WANG X., LIN C.L., et al. 2015. *Significance of particle aggregation in the reverse flotation of kaolinite from bauxite ore*. Minerals Engineering, 78: 58-65.
- LONGHUA X., YUEHUA H., FAQIN D., et al. 2015. *Effects of particle size and chain length on flotation of quaternary ammonium salts onto kaolinite*. Mineralogy and Petrology, 109: 309-316.
- MA C., ABULIKEMU A., BAO J., et al. 2023. *Stacking Order Induced Anion Redox Regulation for Layer-Structured Na<sub>0.75</sub>Li<sub>0.2</sub>Mn<sub>0.7</sub>Cu<sub>0.1</sub>O<sub>2</sub> Cathode Materials*. Small, 19(37): 2302332.
- MA X., BRUCKARD W.J., HOLMES R. 2009. *Effect of collector, pH and ionic strength on the cationic flotation of kaolinite*. International Journal of Mineral Processing, 93(1): 54-58.
- MORSY F.A., EL-SHERBINY S., HASSAN M.S., et al. 2014. *Modification and evaluation of Egyptian kaolinite as pigment for paper coating*. Powder technology, 264: 430-438.
- MÜLLER A.S., JANJIĆ K., SHOKOOHI-TABRIZI H., et al. 2020. *The response of periodontal cells to kaolinite*. Clinical Oral Investigations, 24: 1205-1215.
- SEGALL M.D., LINDAN P.J.D., PROBERT M.J., et al. 2002. *First-principles simulation: ideas, illustrations and the CASTEP code*. Journal of physics: condensed matter, 14(11): 2717.
- ŠOLC R., GERZABEK M.H., LISCHKA H., et al. 2011. *Wettability of kaolinite (001) surfaces – Molecular dynamic study*. Geoderma, 169: 47-54.
- YANG S., FENG Q., QIU X., et al. 2014. *Relationship between flotation and Fe/Mn ratio of wolframite with benzohydroxamic acid and sodium oleate as collectors*. Physicochemical Problems of Mineral Processing, 50.
- ZHANG B., GUO H., DENG L., et al. 2020. *Undehydrated kaolinite as materials for the preparation of geopolymer through phosphoric acid-activation*. Applied Clay Science, 199: 105887.
- ZHOU C., LIU L., CHEN J., et al. 2022. *Study on the influence of particle size on the flotation separation of kaolinite and quartz*. Powder Technology, 408: 117747.